




Spin-momentum locking in optical rectificationP. Moroshkin ^{1,*}, J. Plumitallo,¹ T. Ochiai ², R. Osgood, III ³ and J. M. Xu^{1,4}¹*Brown University, School of Engineering, Providence, Rhode Island 02912, USA*²*Research Center for Functional Materials, National Institute for Materials Science, Tsukuba 305-0044, Japan*³*Army DEVCOM SC, Natick, Massachusetts 01760, USA*⁴*Department of Physics, Brown University, Providence, Rhode Island 02912, USA*

(Received 5 May 2022; accepted 2 August 2022; published 30 August 2022)

Spin-momentum locking is intriguing and observable optically in the surface-plasmon polariton (SPP) waves. Here, we report on its direct electrical detection. In a periodically patterned metallic surface, a circularly polarized light incident in the Y direction generates a unidirectional SPP by spin-momentum locking in the X direction and was detected via optical rectification at the sample edge in the form of a DC voltage or current.

DOI: [10.1103/PhysRevA.106.023521](https://doi.org/10.1103/PhysRevA.106.023521)**I. INTRODUCTION**

Spin is a fundamental degree of freedom in nature and in classical and quantum mechanics. Spin-orbit coupling is at the foundation of a wide variety of intriguing and enabling phenomena found ranging from chiral molecules [1] to quantum biology and to electron conduction in materials, impacting our world as deep as topological insulators [2], as far as bird migration, and as close as cancer and medicine [3,4].

Classical electromagnetic counterparts of spin-orbit coupling in optics can be just as intriguing and provide, for example, unidirectional or helical propagation of light waves [5].

More recent findings were made in a composite electron-light system—surface-plasmon polaritons (SPPs). In particular, it was observed via optical scatterings that a circularly polarized light induces a unidirectional SPP wave propagating along the metal surface [6–8], resembling the system illustrated in Fig. 1. This was theorized as the spin-momentum locking, making use of a particular newly identified or highlighted property of the SPP waves, namely, the extraordinary transverse spin angular momentum corresponding to the helicity of the SPP waveform:

$$\mathbf{S}_{\text{SPP}} = \frac{[\text{Re}(\mathbf{k}_{\text{SPP}}) \times \text{Im}(\mathbf{k}_{\text{SPP}})]}{[\text{Re}(\mathbf{k}_{\text{SPP}})]^2}. \quad (1)$$

Here, the real part of the SPP wave vector \mathbf{k}_{SPP} determining its propagation direction lies in the plane of the metal surface. Its imaginary part is directed orthogonal to the surface and describes the exponential decay of the evanescent wave into the space above. The resulting spin, \mathbf{S}_{SPP} , lies in the surface plane and is orthogonal to the direction of propagation of the SPP wave, as shown in Fig. 1. Mathematically, this relation (1) holds for all evanescent waves. As such, if it is experimentally observable, it may be regarded as universal, although previously un- or under-explored.

For the first experimental validation, an optical method was devised and reported in Ref. [8] where a SPP wave propagating partially along the transverse (or X) direction was excited by a circularly polarized light beam at oblique incidence along the Y direction. The unidirectional SPP wave scattering off an obstacle (e.g., microscopic defects) becomes optically observable via a microscope.

Conditionally, for the process to occur, the photon spin angular momentum, \mathbf{S}_{Las} , determined by its polarization has to match that of the SPP. As a result, the incident laser light can excite the SPP mode that propagates in the direction determined by the handedness of the light polarization.

This work reports that it can be made electrically detectable via a direct measurement of the optical rectification (OR) current induced in an asymmetric metallic grating (gold) by a circularly polarized light. We also show that its polarity switching corresponding to the light polarization handedness change, allowing for applications in electrical detection of chiral objects such as mirror-pairs of molecules—enantiomers, which are otherwise indistinguishable by their scalar physical properties, yet play a critical role in nature and in life.

Optical rectification itself represents an effective and a high-speed alternative to the photodetection by semiconductor diodes, without the limitations due to band gap and finite capacitance. Differing the conventional plasmonic resonance enhanced photon-drag effect, the electron (OR) current under study is in the X direction, orthogonal to the linear momentum of the light incident in the YZ plane. Underlying this system is a set of interesting interplays of field-enhancement, nonlinear light-matter interactions and inversion-symmetry breaking [9–15]. The system could also be viewed as yet another platform for an extension to the mesoscopic scale of the Fermi-liquid theory of metals, in which an “anomalous velocity” of Bloch electrons can be expected, per Karplus and Luttinger [16], in materials or unit cells that are asymmetric in spatial and/or time inversion, and for which direct experimental observations have been sought after [17].

*petr_moroshkin@brown.edu

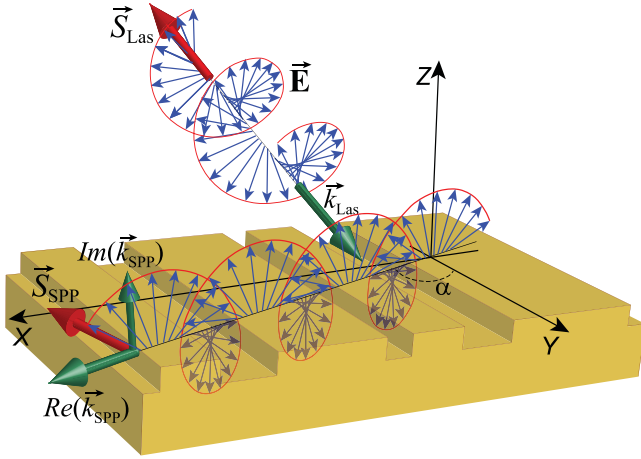


FIG. 1. Conceptual illustration of spin-momentum locked light-matter interaction involving a circularly polarized light wave in air and a SPP wave in a periodically structured metal film.

II. EXPERIMENT

In this work the electrical response of the spin-momentum locking is observed—a photoinduced DC current in a direction transverse to the light incidence is measured at the edges of a periodically patterned gold film on top of a glass substrate. We have investigated the samples with two different patterns of the same period $D = 1488$ nm: symmetric and asymmetric.

The structure of the unit cell of an asymmetric pattern is illustrated in Fig. 2(a). It consists of two ridges or terraces of unequal widths $A_1 = D/2$ and $A_2 = D/5$ placed on top of a continuous gold film with a thickness $H_0 = 100$ nm. The terraces have a height $H_1 = 80$ nm. The grooves or intervals between the terraces have unequal widths $B_1 = D/5$ and $B_2 = D/10$. This design breaks the inversion symmetry along the X direction (across the grating lines) and the SPP excited by the

pump-laser light introduces a second-order optical nonlinearity in a material with a zero $\chi^{(2)}$.

The second structure is shown in Fig. 2(b). It has a unit cell consisting of a single terrace with a width $A_1 = D/2$ and a single groove of the same width. The only difference thus being the absence of the smaller terrace A_2 .

The rectangularly shaped samples have a total length of $446 \mu\text{m}$ along the X direction (300 unit cells) and a width in the Y direction of $200 \mu\text{m}$. They are fabricated by means of electron-beam lithography and a liftoff process. An electron microscope (SEM) image of the fabricated asymmetric grating is shown in Fig. 2(d), next to its cross-sectional view.

Both grating structures allow a much more efficient coupling of the incident light to the SPP excitations in the film than in the prior studies of spin-momentum locking [8] and enable its direct electrical observation by OR.

The schematic of the sample and the experimental setup is shown in Fig. 2. The setup is similar to that described in a separate pursuit of the more conventional OR effect by electron ratchet transport [11] under linear polarization and normal incidence. The grating is illuminated by a cw diode laser with a wavelength $\lambda_{\text{Las}} = 808$ nm and a power $P_{\text{Las}} = 100$ mW focused to a spot $100 \mu\text{m}$ in diameter. The laser beam is tilted by an angle θ with respect to the surface normal in the YZ incidence plane that is parallel to the grooves and ridges, as shown in Fig. 2(e). The photoinduced DC current, i.e., the OR current, is detected along the X direction, orthogonal to the incidence plane and the grooves, hence not entangled with the usual photon-drag effect.

In the experiment we measure the OR currents induced by four different types of the laser polarization: $I_x(P, \theta)$ and $I_x(S, \theta)$ for the linear P and S polarizations; $I_x(L, \theta)$ and $I_x(R, \theta)$ for the left and right circular polarizations, respectively. To measure the relatively weak optical rectification (OR) currents and suppress any thermally induced contributions in the experimental signals, the laser beam is on-off modulated by a mechanical chopper at a frequency of 200 Hz. The OR signal is detected at the modulation frequency with the help of a lock-in amplifier in the current measurement mode, having the input impedance of 1 k Ω . All measurement conditions are kept the same (as much as possible) for each measurement, only the polarization is changed.

Typical photocurrent signals are shown in Figs. 3 and 4. The largest observed photocurrent has a magnitude of ≈ 3 nA. The corresponding energy conversion efficiency from the laser light to the electric current thus reaches $\approx 10^{-13}$, at maximum. Laser illumination of a flat (unpatterned) part of the gold film produces a photocurrent on the order of 10–20 pA, close to the sensitivity limit of our experimental setup.

In Fig. 3(a) we plot the experimental OR signals obtained under the excitation of the asymmetric grating with a linearly polarized light vs the angle of incidence θ . The largest current is achieved at normal incidence, with the laser polarized orthogonal to the grooves of the grating (S polarization). This agrees with the OR by electron ratchet transport in an asymmetric grating under linear polarization. As shown in Ref. [11], under these conditions the laser resonantly excites the SPP mode with a wave vector directed orthogonal to the grooves and ridges of the grating. The projection of \mathbf{k}_{SPP} onto

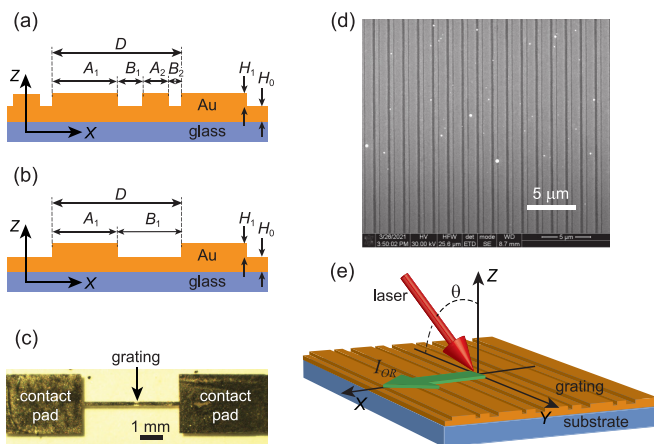


FIG. 2. Schematic sketches of (a) asymmetric and (b) symmetric one-dimensional (1D) grating structures used in the experiment. (c) Microphotograph of the entire sample. (d) Electron microscope (SEM) image of the nonsymmetric grating. (e) Sketch of the experimental setup and light incidence.

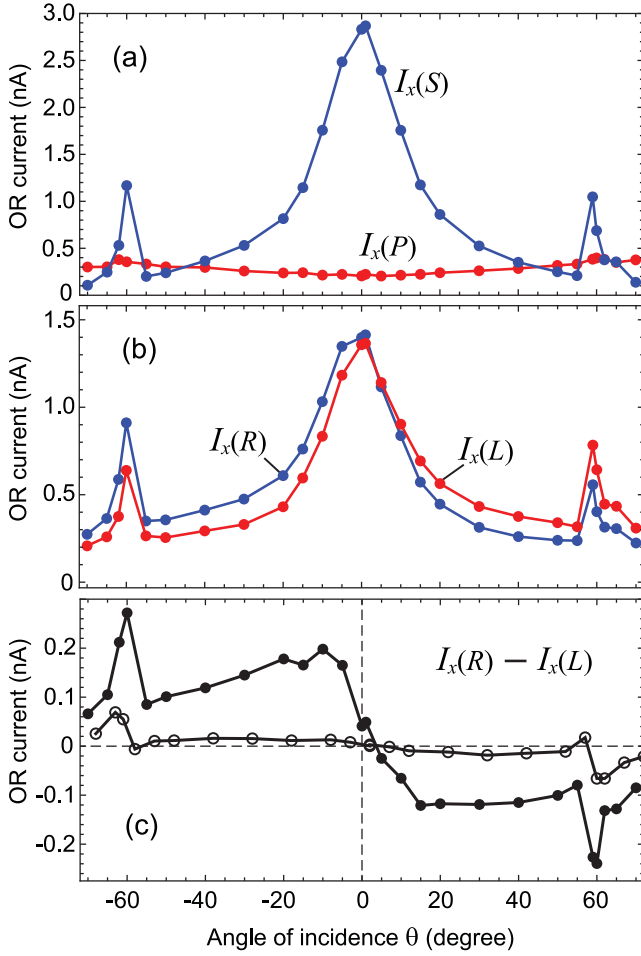


FIG. 3. Experimental OR currents vs the angle of incidence. (a) Excitation of the asymmetric grating by linearly polarized light. Red: P polarization (along the grooves), blue: S polarization (orthogonal to the grooves) for the asymmetric grating. (b) Excitation of the asymmetric grating by circularly polarized light. Red: $I_x(L, \theta)$, blue: $I_x(R, \theta)$, for the asymmetric grating. (c) Helicity-dependent OR current $I_C = I_x(R, \theta) - I_x(L, \theta)$. Filled circles: the asymmetric grating of Fig. 2(a), empty circles: grating with a symmetric unit cell, Fig. 2(b).

the XY plane, \mathbf{K}_{SPP} fulfills the momentum conservation:

$$\mathbf{K}_{\text{SPP}}(\omega_{\text{Las}}) = (\pm 2Q, 0, 0), \quad (2)$$

where Q is the grating “crystal momentum,” $Q = 2\pi/D$.

The two smaller side peaks in $I_x(S, \theta)$ at $\theta \approx \pm 60^\circ$ are attributed to the excitation of SPP waves propagating along the surface at an angle α with respect to the grooves. Their in-plane wave vectors obey the momentum conservation condition and are given by

$$\mathbf{K}_{\text{SPP}}(\omega_{\text{Las}}) = (\pm Q, k_{\text{Las}} \sin \theta, 0). \quad (3)$$

Assuming that the SPP frequency is primarily material dependent, so assuming $|\mathbf{K}_{\text{SPP}}(\omega_{\text{Las}})| \approx 2Q$, Eq. (3) can be fulfilled by setting the SPP propagation angle $\alpha \pm 30^\circ$ from the Y axis, as indicated by the $\text{Re}(\mathbf{k}_{\text{SPP}})$ vector in Fig. 1, and the angle of incidence of the laser beam $\theta \approx \pm 70^\circ$. The deviation is

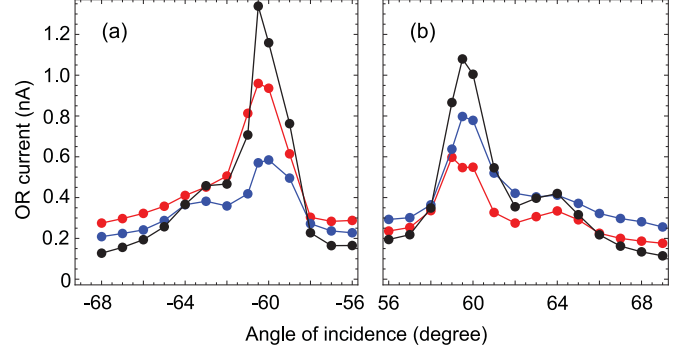


FIG. 4. Experimentally measured OR current at the incidence angle (a) $\theta = -60^\circ$ and (b) $\theta = +60^\circ$. Asymmetric grating. Red curve: RCP, blue: LCP, black: S polarization.

attributable to the dependence of $|\mathbf{K}_{\text{SPP}}(\omega_{\text{Las}})|$ on the propagation angle α .

Higher-resolution scans of these diagonal SPP resonances at $\theta = -60^\circ$ and $\theta = +60^\circ$ are shown in Figs. 4(a) and 4(b), respectively. One can clearly see a partially resolved doublet structure of each resonance that is also found in theoretical curves (see Sec. III).

$I_x(P, \theta)$ measured in the same setup is at a near-zero value, consistent with theory in the next section.

The OR currents excited in the asymmetric grating by the left circularly polarized (LCP) and right circularly polarized (RCP) laser light, respectively, are plotted in Fig. 3(b). The higher-resolution scans of the two diagonal SPP resonances are shown in Fig. 4. The two curves $I_x(R, \theta)$, $I_x(L, \theta)$ strongly resemble that for the $I_x(S, \theta)$, although with a lower absolute value. This is expected since both RCP and LCP can be represented as a sum of the S and P linear polarizations. At normal incidence the measured $I_x(R, \theta)$ and $I_x(L, \theta)$ are practically indistinguishable. However, at $\theta \neq 0$ they differ by 10%–20%.

The difference between $I_x(R, \theta)$ and $I_x(L, \theta)$ can be expected as the SPP waves excited under the spin-momentum locking condition are expected to propagate in different directions, along or against the X direction in which the inversion symmetry is broken. A helicity-dependent or spin-momentum-locking dependent contribution to the OR current I_C is given by the OR current differential: $I_C = I_x(R, \theta) - I_x(L, \theta)$. The dependence $I_C(\theta)$ is plotted in Fig. 3(c). It has an antisymmetric shape, with $I_C(\theta) > 0$ at $\theta < 0$ and $I_C(\theta) < 0$ at $\theta > 0$. In the angular range $10^\circ < |\theta| < 60^\circ$ I_C has a slowly varying magnitude of 100–200 nA. Two sharp peaks at $|\theta| = 60^\circ$ correspond to the diagonal SPP resonances discussed above.

For a symmetric grating, with the laser incident in the YZ plane, one can expect a near-zero rectification current, even under the SPP excitation. Due to the unbroken symmetry, the electron motion in the two opposite directions along the X axis should cancel each other. Our results, in general, confirm this expectation. Under the same conditions, the photocurrent from a symmetric grating is at least 10 times lower than that from the asymmetric one. A detailed study of the differences in OR between the symmetric and asymmetric gratings is beyond the scope of this work. In Fig. 3(c) we plot the $I_C(\theta)$

dependence for the symmetric grating. Despite being several times smaller, I_C in the symmetric grating follows a similar angular dependence as in the asymmetric one. The two diagonal SPP resonance can be seen at the same angle $|\theta| = 60^\circ$ that is determined by the grating period and is independent on the unit-cell profile.

III. THEORY AND NUMERICAL RESULTS

Let us consider the kinetics of the relevant light coupling to the SPP in more detail. The incident plane-wave light $\mathbf{E}^{\text{inc}} = \mathbf{e}_0 \exp(i\mathbf{k}_0 \cdot \mathbf{x})$ induces the Bragg-reflected light, as given by

$$\mathbf{E}^{\text{ref}} = \sum_g \mathbf{r}_g e^{i\mathbf{k}_g^+ \cdot \mathbf{x}}, \quad (4)$$

$$\mathbf{k}_g^\pm = \mathbf{K}_g \pm \Gamma_g \hat{z}, \quad \Gamma_g = \sqrt{k_{\text{Las}}^2 - \mathbf{K}_g^2}, \quad (5)$$

$$\mathbf{K}_g = (g, k_{\text{Las}} \sin \theta, 0), \quad (6)$$

$$\mathbf{r}_g = r_{gp} \mathbf{p}_g + r_{gs} \mathbf{s}_g, \quad (7)$$

$$\mathbf{p}_g = \left(\frac{\Gamma_g}{k_{\text{Las}}} \frac{g}{|\mathbf{K}_g|}, \frac{\Gamma_g}{k_{\text{Las}}} \frac{k_{\text{Las}} \sin \theta}{|\mathbf{K}_g|}, -\frac{|\mathbf{K}_g|}{k_{\text{Las}}} \right), \quad (8)$$

$$\mathbf{s}_g = \left(-\frac{k_{\text{Las}} \sin \theta}{|\mathbf{K}_g|}, \frac{g}{|\mathbf{K}_g|}, 0 \right), \quad (9)$$

where \mathbf{r}_g and \mathbf{k}_g^+ are the amplitude and wave vector, respectively, of the Bragg-reflected light of reciprocal lattice $g = (\text{integer}) \times Q$, Γ_g is the z component of the wave vector either real or pure imaginary, \mathbf{p}_g and \mathbf{s}_g are the P and S polarization vectors, respectively, orthogonal to \mathbf{k}_g^+ , and r_{gp} and r_{gs} are their amplitudes.

In the limit of grazing incidence, the P polarization vector has a spin-momentum locking in the XZ plane. Namely, we have

$$\mathbf{p}_g|_{\theta=\frac{\pi}{2}} = \left(\frac{i|g|}{k_{\text{Las}}} \frac{g}{\sqrt{g^2 + k_{\text{Las}}^2}}, \frac{i|g|}{\sqrt{g^2 + k_{\text{Las}}^2}}, -\frac{\sqrt{g^2 + k_{\text{Las}}^2}}{k_{\text{Las}}} \right). \quad (10)$$

If g changes its sign, the imaginary x component changes its sign, whereas the real z component does not. This property indicates the reversal of the handedness of the elliptic polarization, depending on the sign of g .

Naively, the photocurrent can be generated through the momentum transfer from the incident light to the carriers of the SPP wave in the metal [12,18]. It is expressed as

$$I_x^{\text{MT}} \simeq -W \frac{e\epsilon_0}{2m\gamma k_{\text{Las}}^2} \sum_{g \in \text{open}} g \Gamma_g |\mathbf{r}_g|^2, \quad (11)$$

where e and m are the charge and mass, respectively, of the carriers in the metal, ϵ_0 is the vacuum permittivity, γ is a phenomenological damping, W is the relevant sample size, and the summation over g is limited in the open diffraction channels. We here neglected the transmitted light into the substrate, which is very small compared with reflections. In the experiment, the Bragg reflection channels of nonzero g are closed for $|\theta| \geq 58^\circ$. Thus, the photocurrent vanishes there and the experimental side peaks of the photocurrent around

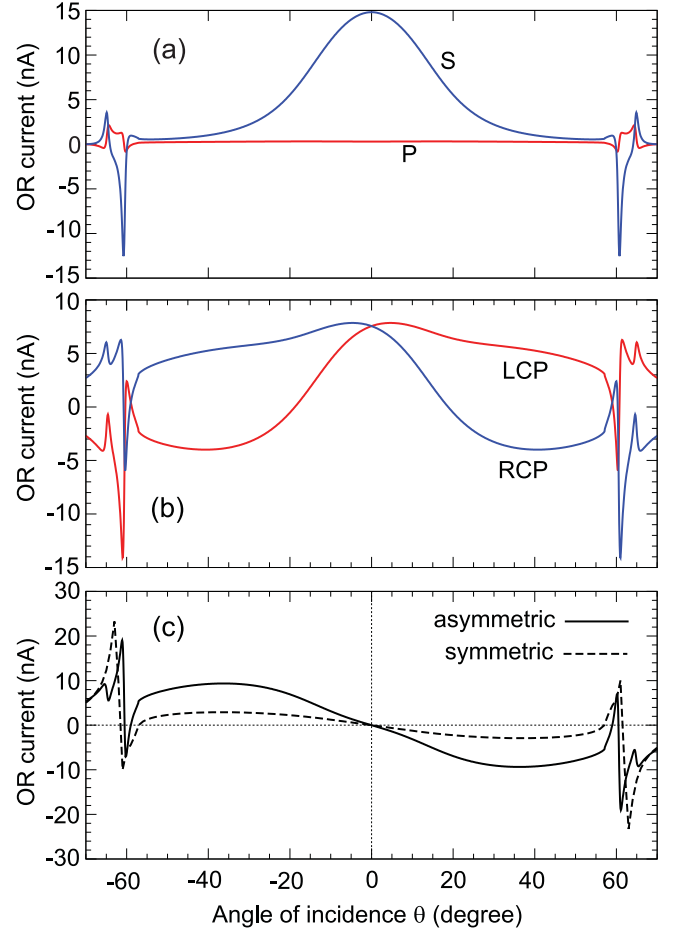


FIG. 5. Theoretical photocurrent averaged over an asymmetric unit cell, as a function of incidence angle. (a) Linear (S and P) polarization of the incident light. (b) Circular (RCP and LCP) polarization. (c) The difference in the photocurrent between RCP and LCP for the asymmetric and symmetric gratings. The geometrical parameters of the grating, the wavelength, and the flux density of the incident light are taken from the experimental values.

$\theta = \pm 60^\circ$ are not described in this relatively simple viewpoint.

To explain the side peaks, we need to take account of near-field effects, which can be substantial and intensified at SPP resonances but are absent in the above momentum-transfer argument. Considering the photocurrent by the local field-force exerted on the carriers via the Maxwell's stress tensor T_{ij} as [18], we have

$$I_x = \frac{e}{m\gamma} \frac{W}{D} \int_0^D dx \int_0^{H(x)} dz \sum_{j=x,y,z} \frac{\partial T_{xj}}{\partial x_j}, \quad (12)$$

$$T_{ij} = \frac{1}{2} \text{Re}[\epsilon_0 E_i^* E_j + \mu_0 H_i^* H_j] - \frac{1}{4} \delta_{ij} (\epsilon_0 |\mathbf{E}|^2 + \mu_0 |\mathbf{H}|^2). \quad (13)$$

Here, $H(x)$ ($=H_0$ or $H_0 + H_1$) is the thickness function of the grating, μ_0 is the vacuum permeability, while \mathbf{E} and \mathbf{H} are the electric and magnetic fields, respectively, of the linear response. We assume the spatial average of the photocurrent over a unit cell for I_x . In the evaluation of Eq. (12), we need

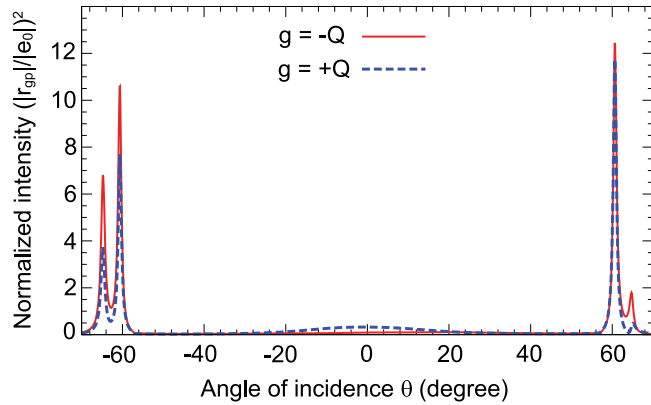


FIG. 6. Calculated normalized intensity of the P -polarized Bragg-reflection channels $|r_{sp}|^2$ of $g = \pm Q$ induced by the LCP light as a function of the incident angle. The intensity by the RCP light is obtained by substituting $\theta \rightarrow -\theta$.

the Bragg-reflected wave at the grating top ($z = H_0 + H_1$), through $\mathbf{E} = \mathbf{E}^{\text{inc}} + \mathbf{E}^{\text{ref}}$. We also need the \mathbf{E} (and \mathbf{H}) field inside the grating, which is available via the rigorous coupled-wave analysis we performed.

Figure 5 shows the theoretical photocurrent angular spectra according to the above formula. Here, the dielectric constant of the substrate is taken to be $\epsilon_s = 2.1$. The following Drude fitting for the dielectric function of gold is assumed: $\epsilon(\omega) = \epsilon_\infty - \omega_p^2/[\omega(\omega + i\gamma)]$ with $\epsilon_\infty = 9.84$, $\hbar\omega_p = 9.01$ eV, and $\hbar\gamma = 0.072$ eV.

The experimental OR current peak of the S polarization at normal incidence and its contrast to the P polarization, which is silent (near zero) there, are reproduced well. Moreover, the side peaks with asymmetric subfeatures are also found in the theoretical angular spectra. This asymmetry suggests an interference among resonant modes. Indeed, we also see the doublet peaks of the two diagonally propagating SPPs of $g = \pm Q$, in the absorption angular spectrum (see Fig. 7 in the Appendix).

Interestingly, the polarity of the OR current is sharply reversed between the two components of each SPP peak doublet near $\theta = \pm 60^\circ$. This sign reversal can be seen in the theoretical curves corresponding to S , RCP, and LCP polarizations (Fig. 5). Our higher-resolution experimental scans (Fig. 4) confirm the doublet structure of each resonance, but show no sign reversal. However, the sharpness and the polarity switching are fragile against defects and damping which are present in the experiments. By varying the magnitude of the damping parameter γ in Eq. (12) and in the Drude model, rounded asymmetric peaks are produced in the model, quite similar to the experimental data (Fig. 9).

The photocurrent satisfies a symmetry relation under Y -coordinate inversion:

$$I_x(P, \theta) = I_x(P, -\theta), \quad (14)$$

$$I_x(S, \theta) = I_x(S, -\theta), \quad (15)$$

$$I_x(L, \theta) = I_x(R, -\theta). \quad (16)$$

Moreover, the photocurrent satisfies a sum rule regarding the polarization:

$$I_x(P, \theta) + I_x(S, \theta) = I_x(L, \theta) + I_x(R, \theta). \quad (17)$$

This sum rule comes from the fact that the photocurrent is bilinear in the electric field. The experimental curves also satisfy these relations.

A clear contrast in the photocurrent regarding the handedness of the circular polarization is observed in Fig. 5(c). The contrast is maximized around the side peaks of the SPPs, but is significant even in the off-resonant regime. The latter is attributed to near-field effects in the optical response, which is absent in the momentum-transfer argument (see also the Appendix) and to the helicity ratchet effect [19,20].

The contrast between LCP and RCP in the side peaks is also observed in the Bragg-reflection amplitudes of $p_{g=\pm Q}$, as shown in Fig. 6.

These Bragg-reflection channels are relevant to the SPP resonance and show that the circular polarization of incident light can excite the diagonally propagating SPP modes of $g = \pm Q$ depending on the handedness. This property also supports photocurrent control by light spin via the spin-momentum locking.

IV. DISCUSSION

Based on the findings from experimental and theoretical analysis, we may now ascribe the observed helicity-dependent OR current as a result of the spin-momentum locking expected of this system. The excitation of a predominantly unidirectional SPP wave, propagating either in the X or in the $-X$ direction, by LCP or RCP light, occurred efficiently under the spin-momentum locking condition [6,7]; e.g., when the spin angular momentum of the evanescent SPP wave, S_{SPP} , matched that of the incident laser light, S_{Las} , as illustrated in Fig. 1. Switching the polarization of the incident light from RCP to LCP or vice versa leads to the reversal of S_{Las} and of the matched S_{SPP} . The latter resulted in the observed selective excitation of SPP waves propagating in opposite directions and therefore the difference in the detected OR current. The same result can be achieved by flipping the incidence angle from $\theta > 0$ to $\theta < 0$, as observed in both our experiments and theoretical modeling.

A closer inspection of Figs. 3 and 5 reveals two distinct contributions to I_C : one is weakly dependent on the angle of incidence in the range of $|\theta| = 10^\circ - 60^\circ$ and another is sharply peaked near $\theta = \pm 60^\circ$. The latter is associated with the excitation of the “diagonal” SPP resonances described by Eq. (3). The corresponding SPP waves propagate in the XY plane at $\alpha \approx \pm 30^\circ$, with the sign depending on the handedness of the incident laser light.

The detailed mechanisms of the helicity-dependent OR current in the range $|\theta| = 10^\circ - 60^\circ$ are more complex given the angular dependence of the intensity absorption (reflection) into (from) the textured surface over this range. $\mathbf{K}_{\text{SPP}}(\omega_{\text{Las}}) = 2Q\hat{x}$ is fulfilled at $\theta = 0$ where I_C equals zero.

An additional symmetry breaking arises from the asymmetric structure of the grating unit cell (Fig. 2). It ensures a significant OR current at most incidence directions, including $\theta = 0$, from the force arising from the asymmetric electro-

magnetic near-field and charge distributions localized and enhanced by the SPP. However, the spin-momentum-locking effect is also expected in a symmetric grating. It is indeed observed, as is demonstrated experimentally in Fig. 3(c) and theoretically in Fig. 5(c), where the second curve is obtained by measuring $I_x(R, \theta) - I_x(L, \theta)$ on a sample with the same period $D = 1488$ nm and a symmetric unit cell.

Overall, the symmetric grating produces a weaker OR current, especially near $\theta = 0$. Nevertheless, one still can distinguish the antisymmetric dependence of $I_C(\theta)$, crossing zero at $\theta = 0$. The two peaks due to the “diagonal” SPP resonances remain well resolved and are $\approx 3\times$ weaker than those from an asymmetric grating in the experiment.

The deviation between experiment and theory are probably from grating imperfections, e.g., disorder and finite size, together with electrode and beam-shape effects. They are not included in the theory. Also, the theory is based on the local response approximation, lacking the nonlocal response which is often critical in metallic micro- and nanostructures. Nevertheless, the essential features are consistent between them.

As noted above, the OR current peaks around $\theta = \pm 60^\circ$ are selectively excited by incident light with the corresponding helicity or handedness. In the linear response, this can be verified as the corresponding absorption peaks. Numerical simulations reveal that these peaks correspond to standing waves whose maxima are in phase and localized to the grating terraces. However, a direct optical detection of the spin-momentum locking would require a conversion process of the relevant evanescent wave of the SPP to a far field via, for instance, a scanning near-field optical microscope tip. This conversion is an extrinsic process and will likely perturb the spin-momentum-locking condition. The electrical detection via the OR does not require such an extrinsic process and the conversion from optical to electric signal is intrinsic and governed by the built-in second-order optical nonlinearity of the SPP wave in the patterned metal film. This nonlinearity is not of the ordinary $P_i = \chi_{ijk}^{(2)} E_j E_k$ type but involves the spatial derivative as $P_i = Q_{ijkl} E_j \partial E_l / \partial x_k$, where P_i is the nonlinear polarization density and the \mathbf{E} field is greatly intensified in the near-field zone of the SPP and is asymmetrically distributed over the mesoscopic unit cell. The derivative term gives rise to a significant plasmonic enhancement. It is interesting and worth noting that the host material gold itself is inversion symmetric and has a zero second-order nonlinearity $\chi_{ijk}^{(2)}$, both of which are essential for optical rectification.

Many intriguing questions are opened by this work. For example, one is the comparison to the single-groove system [8], where an optical detection of the spin-momentum locking was made. In this case, the source of the SPP is localized at the groove. In the case of the grating, many grooves simultaneously become synchronized sources of the SPP, resulting in the interference among the SPPs. Such interferences and light-matter interaction in the strong-coupling regime can enable a number of effects as interesting as the now well-studied phenomena in the epsilon-near-zero regime and as far-reaching as quantum-enhanced plasmonic sensing [21]. In this work, this interference gives rise to a stronger OR signal than in the single-groove case and enables the direct electrical detection of the spin-momentum locking reported here and the strong off-axis resonances at $\pm 60^\circ$. Furthermore,

the inversion-symmetry breaking by the mesoscopic grating and the incidence of circularly polarized light can enhance the controllability of the OR signal, although a detailed investigation of this effect is beyond the scope of the present paper. Other questions including how the second-harmonic generation can be tied to the helicity of the incident light are waiting to be investigated in future efforts.

ACKNOWLEDGMENTS

This material is based upon work supported in part by the U.S. Army Research Office under Contract/Grant No. W911NF-14-2-0075 and No. W911NF-21-1-0181 and by AFOSR, Grant No. FA9550-19-1-0355. We thank Dr. K. Bliokh for the interesting discussions and his interests in research in this direction. We acknowledge the support from JSPS KAKENHI Grant (Japan) No. 22K03488 and from the DEVCOM SC CTO Office (USA).

APPENDIX A: MOMENTUM TRANSFER ARGUMENT

Let us summarize the photocurrent by a simple momentum transfer argument. In this viewpoint, the photocurrent is generated by the momentum transfer from the incident light to the charge carriers. The photocurrent in the plane is given by

$$\begin{aligned} \mathbf{I}_{\parallel}^{\text{MT}} &= W \frac{e\epsilon_0}{2m\gamma k_{\text{Las}}^2} \left(|e_0|^2 \Gamma_0 \mathbf{K}_0 - \sum_{g \in \text{open}} (|r_g|^2 \Gamma_g + |t_g|^2 \Gamma_g^{(s)}) \mathbf{K}_g \right), \end{aligned} \quad (\text{A1})$$

where \mathbf{K}_0 and \mathbf{K}_g are the two-dimensional (2D) momenta of the incident and Bragg-diffracted light, respectively. We

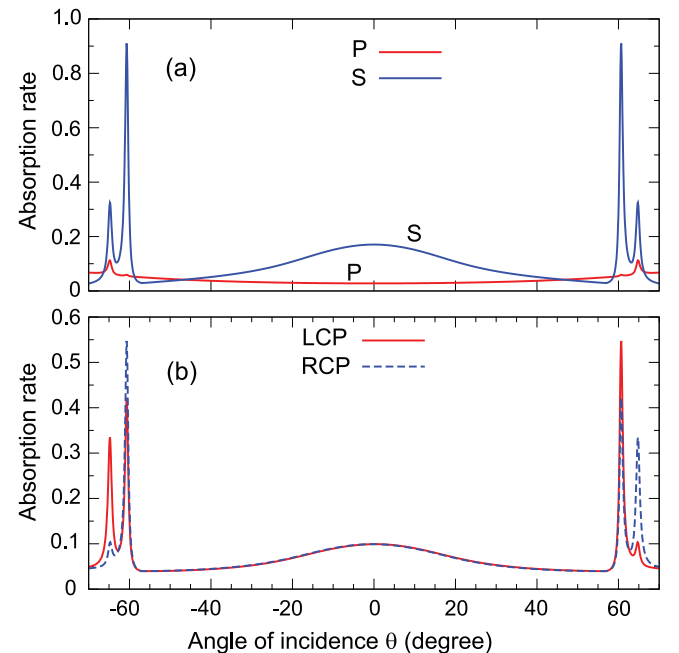


FIG. 7. Calculated absorption rate in the asymmetric grating of Fig. 2 as a function of the incident angle. (a) Linear (S and P) polarization of the incident light. (b) Circular (RCP and LCP) polarization.

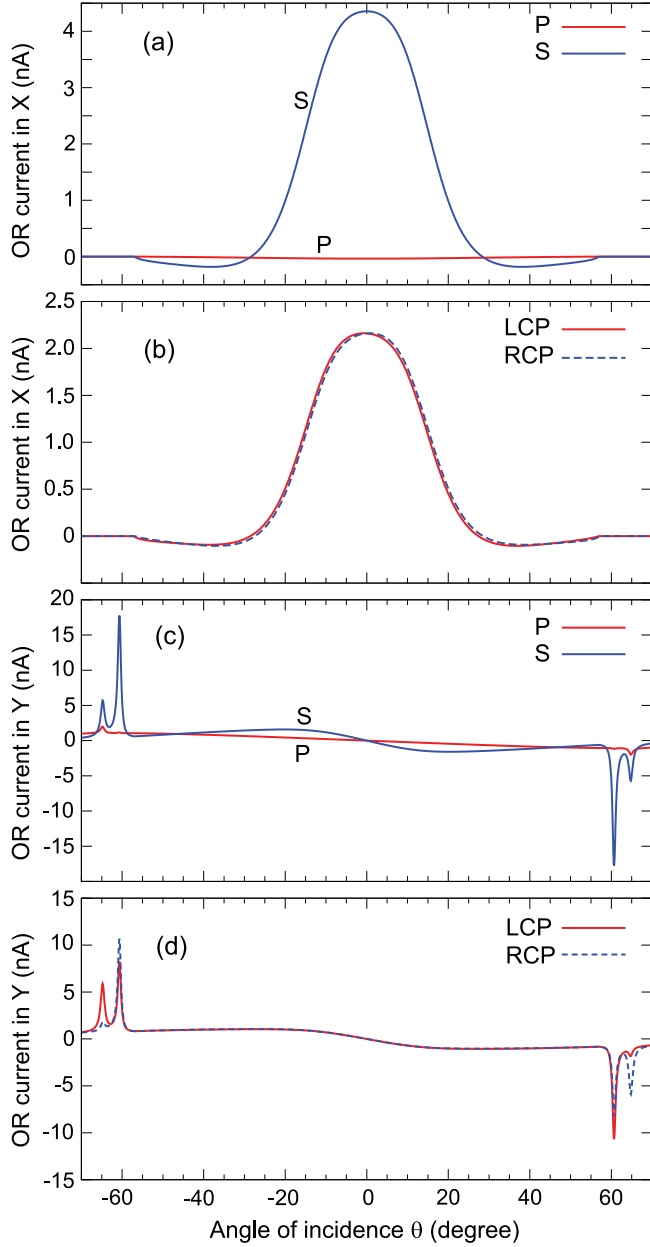


FIG. 8. Calculated transverse and longitudinal photocurrents obtained with the help of the momentum transfer argument.

here take account of the Bragg-transmitted light E^{tra} into the substrate of dielectric constant ϵ_s :

$$\mathbf{E}^{\text{tra}} = \sum_g \mathbf{t}_g e^{i\mathbf{k}_g^{(s)-} \cdot \mathbf{x}}, \quad (\text{A2})$$

$$\mathbf{k}_g^{(s)-} = \mathbf{K}_g - \Gamma_g^{(s)} \hat{z}, \quad \Gamma_g^{(s)} = \sqrt{\epsilon_s k_{\text{Las}}^2 - \mathbf{K}_g^2}. \quad (\text{A3})$$

The weighted difference of the momenta in Eq. (A1) represents the net transferred momentum to the carriers. The expression of the photocurrent is further simplified as

$$I_x^{\text{MT}} = -W \frac{e\epsilon_0}{2m\gamma k_{\text{Las}}^2} \sum_{g \in \text{open}} g (|\mathbf{r}_g|^2 \Gamma_g + |\mathbf{t}_g|^2 \Gamma_g^{(s)}), \quad (\text{A4})$$

$$I_y^{\text{MT}} = W \frac{e\epsilon_0}{2m\gamma} A |\mathbf{e}_0|^2 \cos \theta \sin \theta, \quad (\text{A5})$$

where A is the absorption rate:

$$A = 1 - \sum_{g \in \text{open}} (R_g + T_g), \quad (\text{A6})$$

$$R_g = \frac{|\mathbf{r}_g|^2 \Gamma_g}{|\mathbf{e}_0|^2 \Gamma_0}, \quad T_g = \frac{|\mathbf{t}_g|^2 \Gamma_g^{(s)}}{|\mathbf{e}_0|^2 \Gamma_0}. \quad (\text{A7})$$

In this approach, the transverse photocurrent I_x^{MT} vanishes if the Bragg diffraction channels do not open. Therefore, possible excitation of the SPP in the closed (evanescent) channels is hidden in I_x^{MT} . In contrast, the longitudinal photocurrent I_y^{MT} can exhibit such a signal through the absorption peaks of the SPP.

Figure 7 shows the absorption rate as a function of the incidence angle. It has a broad peak around the normal incidence and double peaks around $\theta = \pm 60^\circ$ of the diagonally propagating SPPs. Since the absorption is bilinear in the electric field, it satisfies a sum rule similar to Eq. (17) regarding the polarization of the incident light.

Figure 8 shows the transverse and longitudinal photocurrents as a function of θ .

As mentioned above, the side peaks around $\theta = \pm 60^\circ$ are not found in the transverse current derived from the momentum transfer argument. Instead, the longitudinal photocurrent exhibits the side peaks. It is also remarkable that the difference in I_x between the LCP and RCP polarizations of the incident light is very small.

APPENDIX B: DAMPING-PARAMETER DEPENDENCE OF THE PHOTOCURRENT

The discrepancy in the photocurrent between the experiment and theory may be attributed to possible imperfections of the grating. Such an imperfection can be described, to some extent, by increasing the Drude damping parameter γ in the dielectric function of gold. Figure 9 shows the photocurrent with increasing γ from the original value.

As the damping parameter is increased, the sharp dips of the asymmetric resonance around $\theta = \pm 60^\circ$ found in the theoretical Fig. 5 are blurred and the negative current region

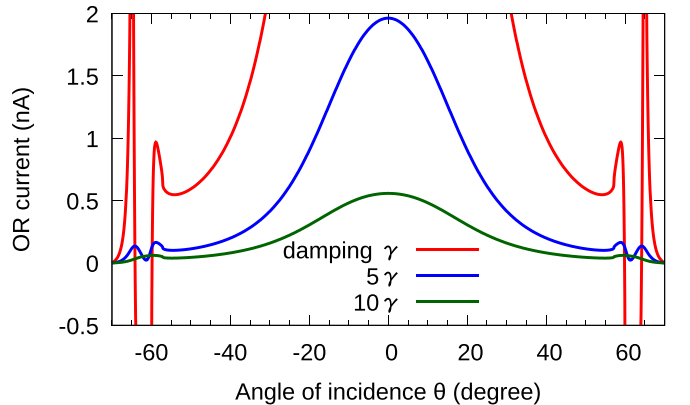


FIG. 9. Calculated transverse photocurrent for the S -polarized incident light, corresponding to different (increased) values of the Drude damping parameter γ . The original γ is taken to be $\hbar\gamma = 0.072$ eV.

tend to disappear in accordance with the experimental curve of Fig. 3(a). It is expected that more elaborated approaches,

such as a two-step relaxation model with a bulk and surface damping, will work to reproduce experimental features.

-
- [1] R. Naaman, Y. Paltiel, and D. H. Waldeck, *Nat. Rev. Chem.* **3**, 250 (2019).
 - [2] M. Z. Hasan and C. L. Kane, *Rev. Mod. Phys.* **82**, 3045 (2010).
 - [3] C. Kerpel, S. Richert, J. G. Storey, S. Pillai, P. A. Liddell, D. Gust, S. R. Mackenzie, P. J. Hore, and C. R. Timmel, *Nat. Commun.* **10**, 3707 (2019).
 - [4] M. Han, M. Xie, J. Han, D. Yuan, T. Yang, and Y. Xiel, *Anal. Bioanal. Chem.* **410**, 2517 (2018).
 - [5] L. Lu, J. D. Joannopoulos, and M. Soljačić, *Nat. Photonics* **8**, 821 (2014).
 - [6] K. Y. Bliokh, D. Smirnova, and F. Nori, *Science* **348**, 1448 (2015).
 - [7] K. Y. Bliokh, F. J. Rodriguez-Fortuno, F. Nori, and A. V. Zayats, *Nat. Photonics* **9**, 796 (2015).
 - [8] F. J. Rodriguez-Fortuno, G. Marino, P. Ginzburg, D. O'Connor, A. Martinez, G. A. Wurtz, and A. V. Zayats, *Science* **340**, 328 (2013).
 - [9] N. Noginova, A. V. Yakim, J. Soimo, L. Gu, and M. A. Noginov, *Phys. Rev. B* **84**, 035447 (2011).
 - [10] A. English, C. W. Cheng, L. Lowe, M. H. Shih, and W. Kuang, *Appl. Phys. Lett.* **98**, 191113 (2011).
 - [11] P. Moroshkin, T. Ochiai, R. Osgood, and J. Xu, *AIP Adv.* **11**, 115006 (2021).
 - [12] T. Hatano, B. Nishikawa, M. Iwanaga, and T. Ishihara, *Opt. Express* **16**, 8236 (2008).
 - [13] N. V. Proscia, M. Moocarme, R. Chang, I. Kretzschmar, V. M. Menon, and L. T. Vuong, *Opt. Express* **24**, 10402 (2016).
 - [14] M. Akbari and T. Ishihara, *Opt. Express* **25**, 2143 (2017).
 - [15] M. Akbari and X. Yang, *Appl. Phys. Lett.* **114**, 171102 (2019).
 - [16] R. Karplus and J. M. Luttinger, *Phys. Rev.* **95**, 1154 (1954).
 - [17] J. E. Moore and J. Orenstein, *Phys. Rev. Lett.* **105**, 026805 (2010).
 - [18] J. E. Goff and W. L. Schaich, *Phys. Rev. B* **56**, 15421 (1997).
 - [19] T. Hatano, T. Ishihara, S. G. Tikhodeev, and N. A. Gippius, *Phys. Rev. Lett.* **103**, 103906 (2009).
 - [20] I. V. Rozhansky, V. Y. Kachorovskii, and M. S. Shur, *Phys. Rev. Lett.* **114**, 246601 (2015).
 - [21] M. Dowran, A. Kumar, B. J. Lawrie, R. C. Pooser, and A. M. Marino, *Optica* **5**, 628 (2018).